ATLAS CONF Note

ATLAS-CONF-2017-026

Search for long-lived, massive particles in events with displaced vertices and missing transverse momentum in $\sqrt{s} = 13$ TeV pp collisions with the ATLAS detector

The ATLAS Collaboration

March 31, 2017

A search for long-lived, massive particles predicted by many theories beyond the Standard Model is presented. The search targets final states with large missing transverse momentum and at least one high-mass displaced vertex with five or more tracks, and uses 32.7 fb^{-1}of $\sqrt{s}$ = 13 TeV pp collision data collected by the ATLAS detector at the LHC. The observed yield is consistent with the expected background. The results are used to extract 95% CL exclusion limits on the production of long-lived gluinos with masses up to 2.2 TeV and lifetimes of $O(10^{-2})$-$O(10)$ ns in a simplified model inspired by Split Supersymmetry.

ATLAS-CONF-2017-026
04 April 2017

1 Introduction

The lack of explanation for the Dark Matter observed in the universe [1], the gauge hierarchy problem [2, 3], and the lack of exact gauge coupling unification at high energies [4] all indicate that the Standard Model (SM) is incomplete and needs to be extended. Many attractive extensions of the SM have been proposed, but decades of searches have set severe constraints on the masses of promptly decaying particles predicted by these models. Searches targeting the more challenging experimental signatures of new long-lived particles (LLPs) have therefore become increasingly important and must be pursued at the Large Hadron Collider (LHC).

A number of beyond-SM (BSM) models predict production of massive particles with lifetimes in the picoseconds to nanoseconds range. These particles would then decay in the inner tracker volume of the experiments at the LHC. The decay products of such particles often contain several electrically charged particles, which can be reconstructed as tracks. If the LLP decays within the tracking volume but at a discernible distance from the interaction point (IP) of the incoming beams, a displaced vertex can be reconstructed by using dedicated tracking techniques.

There are various mechanisms by which particles obtain significant lifetimes in BSM theories. The decays of such particles can be suppressed in so-called Hidden Valley models [5] where large barrier potentials reduce the rate of kinematically allowed decays. Long-lived particles also appear in models with small R-parity violating couplings in Supersymmetry (SUSY) [6, 7]. Finally, decays via a highly virtual intermediate state also result in long lifetimes, as is the case for a simplified model inspired by Split SUSY [8, 9] used as a benchmark model for the search presented here. In this model, the supersymmetric partner of the gluon, the gluino ($\tilde{g}$), is kinematically accessible at LHC energies while the corresponding partner particles of the quarks, the squarks ($\tilde{q}$), have masses that are many orders of magnitude larger. Figure 1 shows pair-production of gluinos decaying to two quarks and the lightest supersymmetric particle (LSP), assumed to be the lightest neutralino ($\tilde{\chi}_1^0$). The $\tilde{g} \to q\bar{q}\tilde{\chi}_1^0$ decay is suppressed as it proceeds via a highly virtual squark. Depending on the scale of the squark mass, the gluino lifetime is picoseconds or longer, which is above the hadronisation time scale. The long-lived gluino, transforming as a colour octet, is expected to hadronise and form a bound colour singlet state with SM particles known as an R-hadron [10]. The lifetime of the constituent gluino determines the location of the decay of the R-hadron which can be detected as a displaced vertex.

This search utilises the ATLAS detector and attempts to reconstruct the decays of massive R-hadrons as displaced vertices (DVs). The vertex reconstruction employed is sensitive to LLP decays occurring

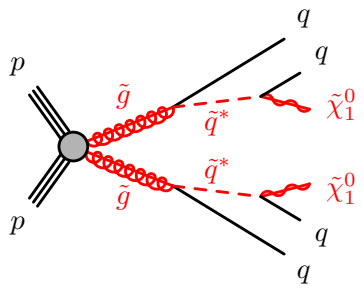

Figure 1: Diagram showing pair-production of gluinos decaying through $\tilde{g} \to q\bar{q}\tilde{\chi}_1^0$. In Split SUSY scenarios, the gluinos are long-lived enough to hadronise to R-hadrons that can give rise to displaced vertices when they decay.

$O(1-100)$ mm from the reconstructed primary vertex (PV), and is sensitive to decays of both electrically charged and neutral states emerging from the PV. The analysis targets final states with at least one DV with a high reconstructed mass and a large track multiplicity, and a large amount of missing transverse momentum (with magnitude $E_{\mathrm{T}}^{\mathrm{miss}}$). In Run 2 of the LHC, the increased centre-of-mass energy gives significant increases in the production cross sections of heavy particles which gives extended sensitivity in mass compared to previous searches. This analysis builds on that of Ref. [11] where the ATLAS collaboration set limits on such processes using 8 TeV pp collisions from the LHC. Decays of new, long-lived particles have been searched for in a variety of experimental settings. These include studies by ATLAS [12–19], CMS [20–25], LHCb [26–29], CDF [30], D0 [31, 32], BABAR [33], Belle [34] and ALEPH [35]. The searches involve a range of experimental signatures, including leptonic [11, 12, 20–22, 24, 30, 31, 33, 35], semileptonic [11, 18, 19, 28], and hadronic final states [11, 16, 17, 23, 25, 26, 32, 33], as well as B-meson decays [27, 29, 33, 34]. Additional techniques make use of non-pointing or delayed photons [13, 14], as well as tracking of the long-lived particle until it decays [15].

The experimental apparatus is described in Section 2, and Section 3 discusses the data set and simulations used for this analysis. The special reconstruction algorithms and event selection criteria are presented in Section 4. Section 5 discusses the sources of backgrounds relevant to this search and the methods employed to estimate the expected yields. The sensitivity to experimental and theoretical uncertainties of the analysis is described in Section 6. Section 7 presents the results and their interpretations.

2 ATLAS detector

The ATLAS experiment [36] at the LHC is a multi-purpose particle detector with a forward-backward symmetric cylindrical geometry and a near 4π coverage in solid angle.[1] The detector consists of several layers of subdetectors. From the IP outwards there is an inner tracking detector (ID), electromagnetic and hadronic calorimeters, and a muon spectrometer (MS).

The ID extends from a radius of about 33 mm to 1100 mm and to $|z|$ of about 3100 mm, and is immersed in a 2 T axial magnetic field. It provides tracking for charged particles within the pseudorapidity region $|\eta| < 2.5$. At small radii, silicon pixel layers and stereo pairs of silicon microstrip detectors provide high-resolution position measurements. The pixel system consists of four barrel layers, and three forward disks on either side of the IP. The barrel pixel layers, which are positioned at radii of 33.3 mm, 50.5 mm, 88.5 mm, and 122.5 mm are of particular relevance to this work. The silicon microstrip tracker (SCT) comprises four double layers in the barrel and nine forward disks on either side. The radial position of the innermost (outermost) SCT barrel layer is 299 mm (514 mm). The final component of the ID, the transition-radiation tracker (TRT), is positioned at larger radii, with coverage up to $|\eta| = 2.0$.

The calorimeter provides coverage over the range $|\eta| < 4.9$. It consists of an electromagnetic calorimeter based on lead and liquid-argon, a hadronic calorimeter comprising a steel and scintillator-tile system in the barrel region and a liquid-argon system with copper and tungsten absorbers in the end caps.

[1] ATLAS uses a right-handed coordinate system with its origin at the nominal IP in the center of the detector and the z-axis along the beam pipe. The x-axis points from the IP to the center of the LHC ring, and the y-axis points upward. Cylindrical coordinates (r, ϕ) are used in the transverse plane, ϕ being the azimuthal angle around the beam pipe. The pseudorapidity is defined in terms of the polar angle θ as $\eta = -\ln\tan(\theta/2)$.

The MS consists of three large superconducting toroids each containing eight coils, a system of trigger as well as precision tracking chambers, which provide trigger and tracking capabilities in the range $|\eta| < 2.4$ and $|\eta| < 2.7$, respectively.

A two-level trigger system is used to select events [37]. The first-level trigger is implemented in custom electronics and uses information from the MS trigger chambers and the calorimeters. This is followed by a software-based high-level trigger system, which runs reconstruction algorithms similar to those used in offline reconstruction. Combined, the two levels reduce the 40 MHz bunch-crossing rate to approximately 1 kHz of events saved for further analysis.

3 Data set and simulated events

The experimental data used in this document are from proton-proton (pp) collisions at $\sqrt{s} = 13$ TeV collected in 2016 at the LHC. After applying requirements on detector status and data quality, the integrated luminosity of the sample corresponds to 32.7 fb^{-1} with an associated uncertainty of ±3.4%, derived using methods similar to those described in Ref. [38].

This search makes use of a number of signal Monte Carlo (MC) samples to determine the efficiency for selecting signal events, and the associated uncertainty. In each sample, gluinos are pair-produced in pp collisions and then hadronised, forming meta-stable R-hadrons which later decay to SM quarks and a neutralino. The mass of the gluino ($m_{\tilde{g}}$) in the simulated samples is set between 400–2000 GeV, its lifetime varies from 0.01 to 50 ns, and the neutralino mass is fixed at 100 GeV. To evaluate signal efficiencies for lifetimes not simulated, available samples are reweighted to different lifetimes. The samples are simulated with Pythia 6.428 [39]. The AUET2B [40] set of tune parameters for the underlying event and the CTEQ6L1 [41] parton distribution function (PDF) set are used. Dedicated routines [10, 42, 43] for hadronisation of heavy coloured particles are used to simulate the production of R-hadrons. The hadronisation process primarily yields meson-like states ($\tilde{g}q\bar{q}$), but baryon-like states ($\tilde{g}qqq$) are predicted as well. In the models used in this analysis, the probability to form a $\tilde{g}g$ state is assumed to be 10%. Following the hadronisation, approximately half of the $\tilde{g}$-based R-hadrons have electric charge, and the charges of the two produced R-hadrons in the event are uncorrelated. The electric charge of the R-hadron is determined by its SM parton content, and while $q = -1$, 0 and 1 dominate, a few percent have double charge. It is worth noting that the vertexing algorithms used in this search (see in Section 4.1) can reconstruct decays of both electrically charged and neutral LLPs produced at the PV.

The cross sections are calculated at next-to-leading order (NLO) assuming a squark mass large enough to completely decouple squark contributions. The most significant contributions to the NLO QCD corrections come from soft-gluon emission of the coloured particles in the initial and final state [44–46]. The resummation of soft-gluon emission is taken into account at next-to-leading logarithmic accuracy (NLO+NLL) [44, 46, 47]. The uncertainty on the cross section predictions are defined as an envelope of the predictions resulting from different choices of PDF sets (CTEQ6.6 [48] and MSTW2008 [49]) and both factorisation and renormalisation scales, as described in Ref. [45]. The nominal cross section is obtained using the midpoint of the envelope.

The ATLAS detector simulation [50] is based on Geant4 [51], and dedicated routines are employed to simulate interactions of R-hadrons with matter [43, 52, 53]. This model assumes the cross section of 12 mb per nucleon for each light valence quark. The per-parton interaction probability is inversely proportional to the squared parton mass, rendering the interactions of the gluinos themselves negligible.

All MC samples include activity from additional pp interactions in the detector, referred to as pileup. The expected minimum-bias interactions that occur in the detector both in-time and out-of-time are generated using Pythia 8.186 [54] and overlaid with the hard-scattering event. Simulated events are reconstructed using the same algorithms used for the collision data. Pythia 6.428 is used to generate the R-hadrons, however it is not expected to give accurate modelling of the initial state radiation (ISR) or final state radiation (FSR). To get a more accurate description of these effects, additional samples of $\tilde{g}\tilde{g}$ production are generated using MadGraph5_aMC@NLO [55], interfaced to the Pythia 8.186 parton shower model, with the A14 [56] set of tuning parameters together with the NNPDF2.3LO [57] PDF set. The distribution of the transverse momentum p_{T} of the $\tilde{g}\tilde{g}$ system simulated with Pythia 6 is reweighted to match the distribution obtained for corresponding MadGraph5_aMC@NLO samples.

4 Reconstruction and event selection

While the focus of this analysis is on dedicated tracking techniques, the entirety of the ATLAS detector is used to reconstruct the jets and $E_{\mathrm{T}}^{\mathrm{miss}}$ in each event giving additional handles on potential signal production. Hadronic jets are reconstructed from calibrated three-dimensional topo-clusters [58] using the anti-k_t jet clustering algorithm [59] with a radius parameter $R = 0.4$. Jet candidates are initially calibrated assuming their energy depositions originate from electromagnetic showers, and then corrected by scaling their four-momenta to the energies of their constituent particles [60–63]. Also electrons, photons, and muons are reconstructed and calibrated, though no explicit requirements are placed on these objects in this search. The $E_{\mathrm{T}}^{\mathrm{miss}}$ is then calculated using all calibrated objects as input as well as those reconstructed tracks not associated with these objects. The latter contribution accounts for potential diffuse, low-p_{T} imbalances [64, 65].

4.1 Reconstruction of displaced tracks and vertices

In the standard ATLAS tracking [66] triplets of hits in the pixel and/or the SCT detectors are used to seed the track finding. By adding further hits along the trajectories, track candidates are fitted and subsequently extrapolated into the TRT. This algorithm places constraints on the transverse and longitudinal impact parameters (d_0 and z_0, respectively) of track candidates with respect to the PV[2]. These constraints result in low efficiency for reconstructing tracks originating from a DV, as such tracks typically have a larger transverse impact parameter than those emerging from the interaction point.

In order to recover tracks from DVs, an additional silicon-seeded *large-radius tracking* (LRT) algorithm pass is performed, using only hits that are not associated with already reconstructed tracks from the standard tracking algorithm. Requirements on the impact parameters are relaxed, allowing tracks to have $|d_0| < 300$ mm and $|z_0| < 1500$ mm, compared to $|d_0| < 10$ mm and $|z_0| < 250$ mm for the first pass. Furthermore, requirements on the number of hits shared by several tracks are slightly relaxed. The tracks from the standard and LRT processing are merged and treated as a single collection in the downstream reconstruction.

To ensure good track parameter measurements, tracks satisfying $p_{\mathrm{T}} > 1$ GeV with at least two associated SCT hits are selected for the DV reconstruction. In order to remove fake tracks, a candidate is discarded if

[2] The PV is required to have at least two associated tracks and satisfy $|z| < 200$ mm. If several exist, the vertex with the largest $\sum(p_{\mathrm{T}}^{\mathrm{track}})^2$ is selected.

it has no TRT hits and fewer than two pixel hits associated. Tracks are also required to have $|d_0| > 2$ mm in order to reject candidates that originate from the PV and a majority of short lived particles, such as b-hadrons. This last requirement ensures the track from an electrically charged LLP will not be associated to the DV.

The DV reconstruction algorithm starts by finding two-track seed vertices from pairs of selected tracks. Seed vertices with a high quality of fit are retained. Both tracks of a seed vertex are required to not have hits in pixel layers at smaller radii than the seed vertex, and to have a hit in the innermost pixel or SCT layer at larger radii. If the seed vertex position is inside or within several millimetres of a tracker layer, hits of that particular layer are neither forbidden nor required. Kinematic requirements on the direction of the vector sum of the momenta of the tracks associated to the seed vertex are applied to make sure it is consistent with the decay of a particle originating from the PV.

At this stage a track can be associated to multiple two-track seed vertices. In order to resolve such ambiguities, an iterative process based on the incompatibility graph approach [67], is applied. After this procedure, each track is associated to at most one seed vertex.

Multi-track DVs are then formed iteratively using the collection of seed vertices. For a given seed vertex V_1, the algorithm finds the seed vertex V_2 that has the smallest value of d/σ_d, where d is the three dimensional distance between V_1 and V_2, and σ_d is the estimated uncertainty on d. If $d/\sigma_d < 3$, a single DV is formed from all the tracks of both seed vertices and the merged vertex is refit. The merging is repeated until no other compatible seed vertices are found. Simultaneously, the association of each track to its vertex is evaluated upon merging, and poorly associated tracks not satisfying additional criteria are removed before the vertex is refitted. This procedure is repeated until no other tracks fail these criteria. Finally, DVs separated by less than 1 mm are combined and refitted. DV candidates are only considered in this search if they fall in the fiducial volume of $R_{\text{DV}} < 300$ mm and $|z_{\text{DV}}| < 300$ mm.

Figure 2 shows the vertex reconstruction efficiency defined as the probability for a true LLP decay to be matched with a reconstructed vertex fulfilling the base vertex selection criteria (described in Section 4.3), in events with a reconstructed PV, as a function of radial position $R_{\text{DV}} = \sqrt{x^2 + y^2}$. The improvement at large radii with respect to the standard tracking is the result of the special LRT processing. The lifetime affects the signal acceptance, but it does not affect the vertex reconstruction efficiency as a function of R_{DV}.

4.2 Material-dominated regions and the effect of disabled detector modules

An important background in any search for displaced vertices comes from hadronic interactions in material-rich regions of the detector [68]. In order to suppress this background, a map defining regions with known material is constructed by studying the positions of vertices in $\sqrt{s} = 13$ TeV minimum bias data. The map is used in the vertex selection to reject vertices within the material regions. The binary veto map is constructed using the observed positions of high vertex-density regions. In these studies, the vertices from the long-lived SM hadrons K^0_S and Λ^0 are vetoed by discarding vertices which match their expected track multiplicities and reconstructed masses. The application of the map-based veto significantly reduces the contribution from hadronic interactions at the cost of discarding approximately 42% of the fiducial volume. The material map is visualised in Figure 3. The locations of the observed vertices failing this veto are projected onto the x-y and R-z planes.

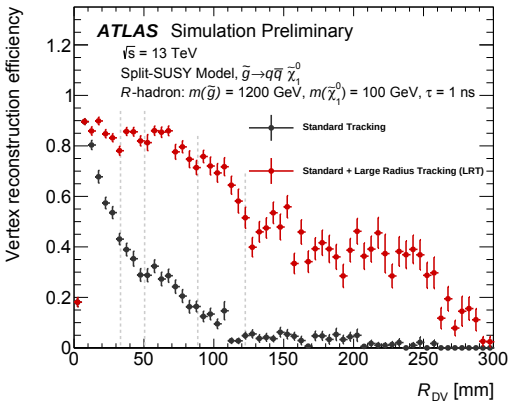

Figure 2: Vertex reconstruction efficiency as a function of its radial position R_{DV}. The efficiency is defined as the probability for a true LLP decay to be matched with a reconstructed vertex fulfilling the base vertex selection criteria, in events with a reconstructed primary vertex. The efficiencies with and without the special LRT processing are shown for one benchmark signal.

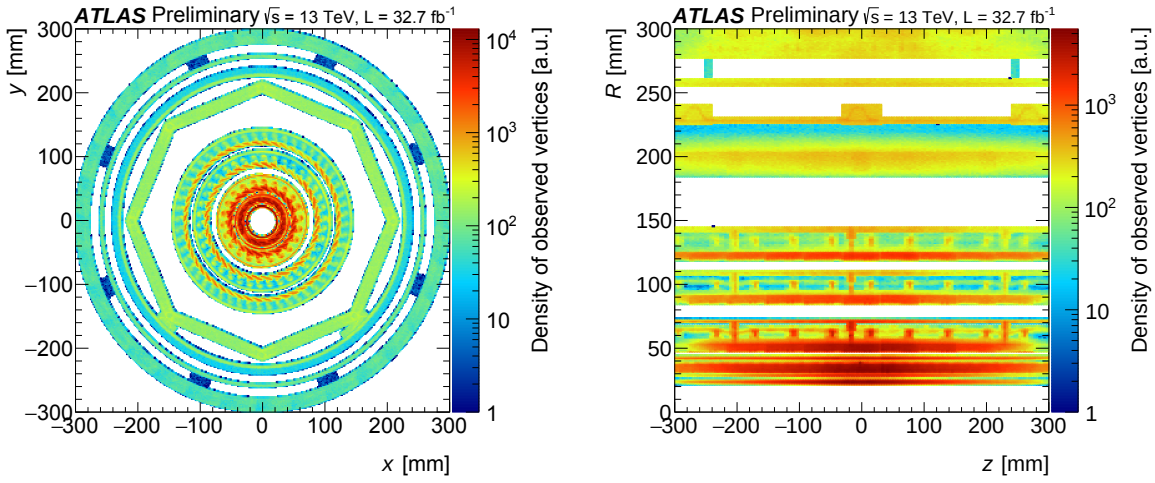

(a) (b)

Figure 3: Two-dimensional maps of the observed vertex density in regions vetoed by the material map, projected in the (a) x-y plane and (b) R-z plane.

In addition to the material veto map, a veto is applied to reject vertices in regions sensitive to the effect of disabled pixel modules. This requirement discards 2.3% of the total fiducial volume.

4.3 Event and vertex selections

All events used in this analysis must satisfy the following selection requirements. Firstly, a subset of the data recorded in 2016 was filtered out during prompt reconstruction throughout the year and was made available in raw data format in order to facilitate the special processing with dedicated track and vertex reconstruction required by this analysis as described below. This filtering included passing a $E_{\mathrm{T}}^{\mathrm{miss}}$, multijet, or single-lepton trigger. For the $E_{\mathrm{T}}^{\mathrm{miss}}$-triggered events used in the signal region (SR) of this search, a requirement on a quantity similar to $E_{\mathrm{T}}^{\mathrm{miss}}$, but using clusters of energy deposited in the calorimeter calibrated assuming they all come from hadrons, was also imposed. The filtering of the first 75% of the data set also required the presence of one trackless[3] jet with $p_{\mathrm{T}} > 70$ GeV or two trackless jets with $p_{\mathrm{T}} > 25$ GeV, and hadronic $E_{\mathrm{T}}^{\mathrm{miss}} > 130$ GeV. For the last 25% of the data set, the trackless jet requirement was removed and hadronic $E_{\mathrm{T}}^{\mathrm{miss}} > 180$ GeV was required instead. The MC events used in this analysis were processed separately in two sub-samples with sizes proportionate to the integrated luminosity of the two data samples.

Additional detector-level quality cuts are applied, vetoing events that are affected by calorimeter noise, corruption, or other effects occurring at the time the data were recorded. Events are required to have at least one PV. To mitigate the contamination of high-$E_{\mathrm{T}}^{\mathrm{miss}}$ events from non-collision background (NCB) processes, additional quality criteria are placed on the leading jet in each event. These requirements use the longitudinal calorimeter-sampling profile of these jets to select for high-p_{T} hadronic activity originating within the detector volume and reduce NCB contributions to at most roughly 10%. Together with the requirement that such events contain a DV candidate, these criteria are called the *event pre-selection* and define the control region (CR).

To further improve signal sensitivity, the *full event selection* criteria that define the SR require that the event be recorded by a $E_{\mathrm{T}}^{\mathrm{miss}}$ trigger and satisfy $E_{\mathrm{T}}^{\mathrm{miss}} > 250$ GeV. This last requirement ensures that the events are in the plateau of the efficiency turn-on curve for both the $E_{\mathrm{T}}^{\mathrm{miss}}$ trigger and the requirement on the $E_{\mathrm{T}}^{\mathrm{miss}}$ based only on clusters described above.

The DV candidates are required to satisfy the following conditions, referred to as the *base vertex selection*:

1. The vertex position must be within the fiducial volume $R_{\mathrm{DV}} < 300$ mm and $|z_{\mathrm{DV}}| < 300$ mm.
2. The vertex must be separated by at least 4 mm in the transverse plane from all reconstructed PVs
3. The vertex must not be in a region that is material-rich or affected by disabled detector modules, as described in Section 4.2.
4. The vertex fit must have $\chi^2/N_{\mathrm{DOF}} < 5$.

These base vertex selection criteria ensure high quality measurements of the vertex properties and reduce the number of vertices from instrumental effects. Vertices passing these criteria are used in the background estimation. For the *final vertex selection* used in the SR of this search, the vertices are required to have at least five associated tracks and a reconstructed invariant mass $m_{\mathrm{DV}} > 10$ GeV. These stricter requirements

[3] A jet is considered trackless if $\sum p_{\mathrm{T}}^{\mathrm{track}} < 5$ GeV, where the sum is taken over all tracks matched to both the PV and the jet.

allow the use of vertices with lower mass and 3-4 tracks for building and validating background estimates, and give a low-background search with good signal sensitivities for a large part of the parameter space for the models of interest.

For models with $m_{\tilde{\chi}_1^0} = 100$ GeV and $\tau = 1$ ns, the search presented here attains an acceptance times efficiency ($\mathcal{A} \times \varepsilon$) of as much as $\sim 40\%$ at $m_{\tilde{g}} = 1.8$ TeV. $\mathcal{A} \times \varepsilon$ is reduced for lower gluino masses: $\sim 25\%$ at $m_{\tilde{g}} = 1.0$ TeV.

5 Background processes and their estimated yields

Given the requirements on the mass ($m_{\text{DV}} > 10$ GeV) and track multiplicity ($n_{\text{tracks}} \geq 5$) placed on the DV candidates in the SR, there is no irreducible background from SM processes. The entirety of the background expected for this search is instrumental in origin. Three sources of such backgrounds are considered in the analysis. Hadronic interactions can give rise to vertices far from the interaction point, especially where there is material in the detector, support structures and services. Decays of short-lived SM particles can occur close to each other and be combined into high-mass vertices with large track multiplicities, in particular in the regions closest to the beams. Finally, low-mass vertices from decays of SM particles or hadronic interactions can be promoted to higher mass if accidentally crossed by an unrelated track at a large angle. Each source of background is estimated with a dedicated method, and is separately evaluated in 12 radial detector regions divided approximately by material structures in the ID volume within the fiducial region.

To retain a large number of vertices, the methods below are applied on events passing the pre-selection. To obtain a final estimate for the SR, an additional *event selection transfer factor* $\epsilon_{\text{SR}} = [5.1 \pm 2.5] \times 10^{-3}$ is applied. This factor is determined by measuring the efficiency of the full event selection with respect to the pre-selection. The events used for calculating ϵ_{SR} are required to have a DV candidate satisfying the base vertex selection. This method relies on the assumption that the mass and track multiplicity distributions of the DVs do not depend on the quantities used in the event selection, which was demonstrated in data to hold within uncertainties. An additional factor κ is used to account for the potential effect of obtaining multiple vertices per event, but this is found to be consistent with 1.0 for the region of vertex properties probed in this search.

5.1 Hadronic interactions

As discussed in Section 4, the bulk of the hadronic interactions occur in detector regions with dense material, and these are rejected using the material map as described above. However, residual hadronic interactions may survive the selections, either due to imperfections in the material map or from interactions with gas molecules in regions without solid material. The low mass region of the m_{DV} distribution is dominated by hadronic interactions, therefore to estimate this background, the m_{DV} distribution in the region $m_{\text{DV}} < 10$ GeV is fit to an exponential distribution and extrapolated to the SR $m_{\text{DV}} > 10$ GeV. The assumptions made by this method and the related uncertainties are discussed in Section 6.

5.2 Merged vertices

The high density of vertices at small radii and the last step of the DV reconstruction, where vertices are combined if they are separated by less than 1 mm, could merge two vertices with low masses and track multiplicities to a single one with significantly higher mass and track multiplicity. To quantify this contribution, vertices from distinct events are randomly merged. The distribution of the distance $d(\mathrm{V}_1, \mathrm{V}_2)$ between two 2-track or 3-track vertices V_1 and V_2 is studied in two samples. To obtain a large sample of reference vertex pairs, one sample is constructed from vertices taken from different events. This sample is then compared to the sample constructed only from pairs of vertices appearing in the same event. Each of the vertices in these pairs is required to satisfy the base DV selection criteria, and their combined mass is required to be greater than 10 GeV. The resulting distributions are shown in Figure 4 for (a) pairs of 2-track vertices (2+2) and (b) for the case of a 2-track vertex paired with a 3-track vertex (2+3). To extract an estimate of the number of vertices merged during DV reconstruction, the different-event distribution is normalised to the same-event distribution in the region $d(\mathrm{V}_1, \mathrm{V}_2) > 1$ mm, and the estimated contribution from merged vertices is given by the scaled template's integral for $d(\mathrm{V}_1, \mathrm{V}_2) < 1$ mm.

It was found that the z positions of vertices in the same-event sample are correlated, since vertices are likely coming from the same hard scatter primary vertex. Naturally, this effect is absent in the different-event sample. As a result, the distributions of the longitudinal distance between the vertices in the model and the same-event samples differ by up to 30% at low values of $d(\mathrm{V}_1, \mathrm{V}_2)$. To correct for this difference between the two samples, the vertex pairs in the different-event sample are reweighted to match the distribution of distances in z of the same-event sample before the yield for $d(\mathrm{V}_1, \mathrm{V}_2) < 1$ mm is extracted. After applying the weights, the model distribution of the three-dimensional distance $d(\mathrm{V}_1, \mathrm{V}_2)$ agrees well with that of the same-event sample in the studied range of $d(\mathrm{V}_1, \mathrm{V}_2) < 120$ mm. This reweighting procedure is applied in the distributions shown in Figure 4.

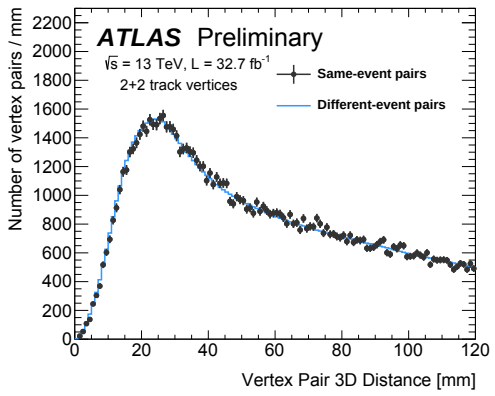

(a) Distances between pairs of two-track vertices

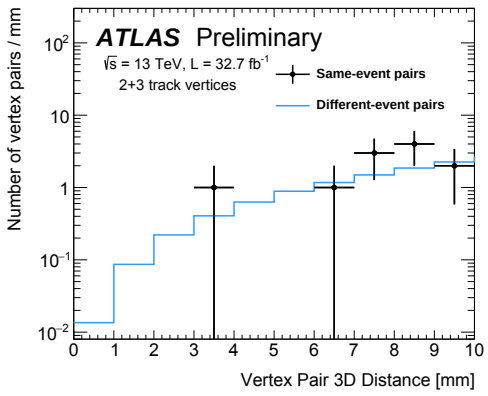

(b) Close-up of the low-distance part of the (2+3) pairs

Figure 4: Distributions of inter-vertex distances in reweighted pairs of vertices passing the base vertex selection in CR events. The same-event (black markers) and different-event (blue histogram) samples are shown for (a) pairs of two-track vertices, and (b) the low-distance part of the (2+3)-pair combinations. The model yield for inter-vertex distance lower than 1 mm gives the prediction for the vertices in the high-mass region resulting from merging during vertex reconstruction.

The background from merged vertex pairs with $d(V_1, V_2) < 1$ mm and $n_{\text{tracks}} \geq 5$ tracks is estimated from vertex pairs where one vertex has two tracks and the other has three tracks. This background is found to be orders of magnitude smaller than the accidental-crossing background discussed below. The background from the merging of two 3-track vertices or a 2-track and a 4-track vertex is determined to be negligible compared to other sources for higher track multiplicities.

5.3 Accidental crossing of vertices and tracks

The final and dominant source of background in the SR for this search is low-mass vertices crossed by an unrelated track in the event. It is not uncommon for such crossings to occur at large angles with respect to the *distance vector* that points from the PV to the DV. This significantly increases the mass of the vertex. In order to estimate the contribution of this effect, (n+1)-track vertices are constructed by adding a *pseudo-track* to n-track vertices from the data in the CR. The pseudo-track is given track parameters drawn randomly from track templates, extracted separately for each radial detector region. These templates are constructed using all tracks associated with DV candidates satisfying $n_{\text{tracks}} \geq 3$ and $m_{\text{DV}} > 3$ GeV found in CR events. The templates contain the track p_{T}, η, and relative azimuthal angle $\Delta\phi$ with respect to the distance vector. In order to model the effect of high-angle crossings, pseudo-tracks drawn from the templates are required to be at an angle larger than $\sqrt{(\Delta\eta)^2 + (\Delta\phi)^2} = 1$ with respect to the distance vector.

To normalise the prediction from the model constructed by this method, the probability of associating an accidentally crossing track to the vertex is extracted by comparing the sample of 3-track vertices seen in the data to the (2+1)-track vertices from the model in the $m_{\text{DV}} > 10$ GeV region. This probability is referred to as the *crossing factor* and is extracted separately for each radial detector region. Figure 5 shows the resulting (2+1)-track predictions from the model along with the 3-track vertices in CR data for two selected radial regions. The observed differences in shape between the model and the data are used in Section 6 to assess an uncertainty on the background estimates from the model.

5.4 Validation of background estimation techniques

To ensure that the methods described above reliably model the backgrounds, two validation regions are constructed to test their predictions. The two regions are designed to be free from significant contamination of any signal considered in this analysis that has not been excluded by previous searches. In the low-$E_{\text{T}}^{\text{miss}}$ validation region, denoted VRLM, the performance of these methods for vertices with exactly 4 tracks is studied as an intermediate point between the 3-track control sample and the $\geq$ 5-track SR. The VRLM event selection requires $E_{\text{T}}^{\text{miss}} < 150$ GeV and that the minimum azimuthal angle between the $E_{\text{T}}^{\text{miss}}$ and all reconstructed jets, $\Delta\phi_{\text{min}}(E_{\text{T}}^{\text{miss}}, \text{jets})$, is less than 0.75. These requirements sufficiently reduce the contribution from the considered signal processes that are not excluded by previous searches [11]. The background estimate extracted from the CR is scaled to account for the efficiency of the $E_{\text{T}}^{\text{miss}}$ and $\Delta\phi_{\text{min}}(E_{\text{T}}^{\text{miss}}, \text{jets})$ requirements to predict the background in VRLM. Since studies in data show that the m_{DV} and n_{tracks} distributions are independent of these event-level quantities, this efficiency factor ϵ_{VRLM} is extracted in a sample with 3-track vertices and applied to the 4-track prediction. This efficiency is found to be $\epsilon_{\text{VRLM}} = [56 \pm 6]\%$.

Additional validation of the background estimation methods is done in a material-enriched validation region, VRM. Here, vertices satisfying the base vertex selection criteria, with the exception of the material

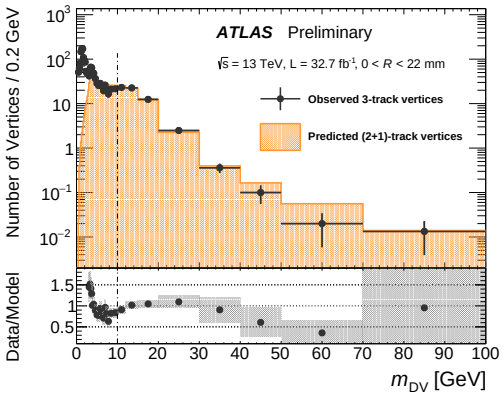

(a) Inside the beam pipe ($R < 22$ mm)

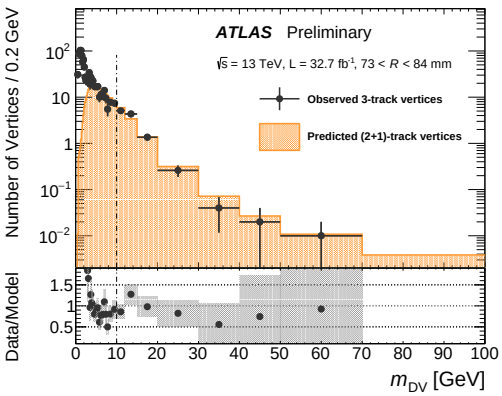

(b) Inside layer 1 (73 mm $< R <$ 84 mm)

Figure 5: Distributions of m_{DV} for 3-track vertices in the CR data for two radial regions, along with the normalised predictions from the track-association method. The spectra from the model are normalised to the data in the $m_{\mathrm{DV}} > 10$ GeV region, and the scaling needed is extracted and used as the crossing factors used to calculate the predictions for higher track multiplicities. The error bars and the grey bands in the bottom ratio distributions represent the statistical uncertainties. The region below 10 GeV is not expected to be described by the accidental-crossing model.

veto which is inverted, are studied. Due to the abundance of hadronic interactions in this region, it contains many more vertices than VRLM. Since accidental-track crossings also happen to vertices from hadronic interactions, this region can be used to validate the estimates for this contribution to vertices in regions not dominated by material. An independent set of crossing factors are derived and applied in this validation region, and their values are found to be similar to those extracted in the samples where the material-rich regions are vetoed.

In both VRLM and VRM, the yields predicted by the background estimation methods are shown in Table 1.

5.5 Final expected yields

The predicted background yields in the various selections are listed in Table 1. The yields are shown separately for each of the estimation methods along with the total for each region. Also shown is the final expected yield in the SR after the application of the scaling factors described above. The total SR prediction from the sum of all background sources is 0.02 ± 0.02, where the total uncertainty includes those of both statistical and systematic origin.

6 Uncertainties

The estimation of the hadronic interactions as described in Section 5 relies on the assumption that the mass spectra of such contributions follow an exponential shape. This assumption is tested using interaction vertices in the GEANT4-based simulations described in Section 3. Based on studies of the deviations from an exponential shape seen in the simulation, an uncertainty of -100% and $+300\%$ is applied to the

Table 1: The number of estimated background vertices with a mass $m_{\text{DV}} > 10$ GeV for the vertex selections used in the control and validation regions are shown. The $(n + 1)$-track contributions are estimated using the accidental-crossing factor method (Section 5.3), the $(2 + i)$-track contribution is obtained from merged vertices (Section 5.2), and the pure n-track estimation is evaluated using the hadronic interactions (Section 5.1). The control region yield is normalised to data. Also shown are the estimated background event yields in the pre-selection region with at least 5 tracks. The predicted background event yield in the signal region appears in the bottom row and includes the transfer factors shown. When two uncertainties are shown, the first is statistical while the second is systematic. When one number is given, it represents the combined uncertainty.

Selection	Sub-Region	Category	Yield
Event pre-selection $n_{\text{trk}} = 3,\ m_{\text{DV}} > 10$ GeV		Measured total	3093
Event pre-selection $n_{\text{trk}} = 4,\ m_{\text{DV}} > 10$ GeV	VRLM	$(3 + 1)$-track	$12.6 \pm 0.3 \pm 1.1$
		$(2 + 2)$-track	3.6 ± 3.6
		Pure 4-track	0.3 ± 0.9
		Sub-total	16 ± 4
		Total (after scaling by ϵ_{VRLM})	**9 ± 2**
	VRM	$(3 + 1)$-track	$137 \pm 3 \pm 30$
		Pure 4-track	16 ± 47
		Total	**150 ± 60**
Event pre-selection $n_{\text{trk}} \geq 5,\ m_{\text{DV}} > 10$ GeV	5-tracks	$(4 + 1)$-track	$1.30 \pm 0.07 \pm 0.12$
		$(2 + 3)$-track	0.01 ± 0.01
		Pure 5-track	0.9 ± 2.8
		Total	**2.2 ± 2.8**
	6-tracks	$(5 + 1)$-track	$0.37 \pm 0.03 \pm 0.04$
		Pure 6-track	0.2 ± 0.6
		Total	**0.6 ± 0.6**
	≥ 7-tracks	$(n + 1)$-track	$0.37 \pm 0.03 \pm 0.04$
		Pure ≥ 7-track	1 ± 3
		Total	**1 ± 3**
	Total		**4.2 ± 4.1**
Full SR selection	**Total** (after scaling by $\epsilon_{\text{SR}} \times \kappa$)		**0.02 ± 0.02**

component of the total background from hadronic interactions. The size of this uncertainty is taken as the largest deviation observed in all track multiplicities for vertices with $m_{\mathrm{DV}} > 10$ GeV in simulation.

The background in the SR due to merged vertices is estimated to be very small with respect to the total background. By comparing the same-event data and different-event model for (2+3)-track vertex pairs, the largest statistically significant discrepancy in any bin in the studied range was observed to be 60%. To be conservative, the systematic uncertainty for this subdominant background is taken to be 100%.

Uncertainties associated with the contribution from low-mass vertices crossed accidentally by an unrelated track are dominated by the uncertainty of the extracted crossing factors. By varying the choice of m_{DV} threshold used for the normalisation of the spectra from the background model by ±5 GeV (with respect to the nominal 10 GeV), an uncertainty is extracted. Since the crossing factors are derived and applied separately for each radial detector region, their uncertainties are as well. The size of the resulting uncertainty for the accidentally crossing track contributions is 10-20% depending on the radial detector region.

Finally, the event selection transfer factor ϵ_{SR} and event-to-vertex level correction κ as described in Section 5 also have associated uncertainties. Both of these uncertainties are derived from varying the kinematic requirements for the vertices and events. Varying the event-level requirements from the pre-selection to the full event selection gives a 50% uncertainty on ϵ_{SR}. Varying the vertex-level requirements in such events gives rise to an additional 16% uncertainty for κ. Since these factors are applied to all background contributions to obtain a final SR estimate, these uncertainties propagate directly to the final estimate.

While the background uncertainties and expectations are derived from data, additional modelling uncertainties that only affect the signal efficiencies are considered and derived from varying parameters used in the simulation and reconstruction. The effect on the signal efficiency due to variations on the amount of simulated pileup is a few percent effect for signal samples considered here. To estimate the size of the uncertainty due to ISR modelling, the size of the reweighting of Pythia 6 to MadGraph5_aMC@NLO as described in Section 3 is taken as an additional systematic uncertainty. This effect corresponds to an uncertainty of a few percent on the signal efficiency for all models considered in this note. The uncertainty on the signal efficiency due to variations in the track and vertex reconstruction efficiency is determined to be $5 - 10$%. Additional uncertainties involving the reconstructed jet energy scale and resolution, as well as the reconstruction of the $E_{\mathrm{T}}^{\mathrm{miss}}$, are evaluated and found to be negligible with respect to the leading uncertainties. No additional uncertainty is considered for the modelling of the production of R-hadrons and their interactions with matter. Decays from both electrically charged and neutral LLPs are reconstructed as displaced vertices in the ID with similar efficiencies, so this search is less sensitive to the fraction of charged states after hadronisation compared to those based on direct-detection signatures. Since the amount of material traversed before a decay in the ID is small, the sensitivity to uncertainties on the per-parton cross section for hadronic interactions is negligible.

7 Results

The final yields for all regions used in this analysis can be found in Table 2. The observed yields are consistent with the background expectation for the validation regions where VRLM contains 9 vertices (9 ± 2 expected) and VRM contains 177 vertices (150 ± 60 expected). The two-dimensional distribution of m_{DV} and track multiplicity is shown for events that satisfy the full event-level selection in Figure 6. The

Table 2: The observed number of vertices for the control and validation regions are shown along with the background expectations for the 32.7 fb^{-1}of data. The last row shows the expected and observed signal region event yields.

Selection	Sub-Region	Estimated	Observed
Event pre-selection $n_{\text{trk}} = 3,\ m_{\text{DV}} > 10$ GeV			3093
Event pre-selection $n_{\text{trk}} = 4,\ m_{\text{DV}} > 10$ GeV	VRLM	**9 ± 2**	**9**
	VRM	**150 ± 60**	**177**
Event pre-selection $n_{\text{trk}} \geq 5,\ m_{\text{DV}} > 10$ GeV	5-tracks	**2.2 ± 2.8**	**1**
	6-tracks	**0.6 ± 0.6**	**1**
	≥7-tracks	**1 ± 3**	**3**
	Total	**4.2 ± 4.1**	**5**
Full SR selection	**Total**	**0.02 ± 0.02**	**0**

final SR yields are highlighted, with 0 events observed (0.02 ± 0.02 expected) in 32.7 fb^{-1}of data from 2016.

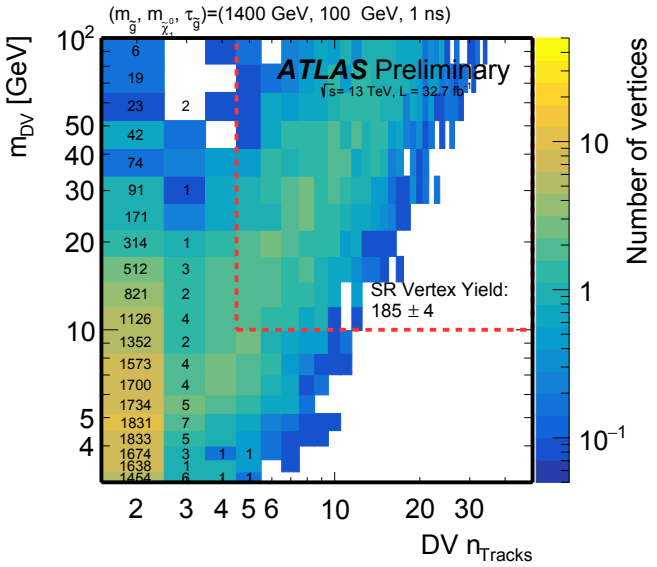

Figure 6: The two-dimensional distribution of m_{DV} and track multiplicity is shown for DVs in events that satisfy all signal region event selection criteria. Drawn numbers correspond to the observations in data, while the colour-representation shows an example distribution for an R-hadron signal with $(m_{\tilde{g}}, m_{\tilde{\chi}_1^0}, \tau)$=(1400 GeV, 100 GeV, 1 ns) used as a benchmark in this search. The dashed line represents the boundary of the signal region requirements.

In the absence of a statistically significant excess in the data, exclusion limits are placed on R-hadron models. These 95% confidence-level (CL) upper limits are calculated using the CL_s prescription [69] with the profile likelihood used as the test statistic, using the HistFitter [70] framework with pseudo-

experiments. Upper limits on the cross section for gluino pair-production as a function of gluino lifetime are shown in Figure 7 for some example values of $m_{\tilde{g}}$ and $m_{\tilde{\chi}_1^0} = 100$ GeV. Also shown are the signal production cross sections for these gluino masses.

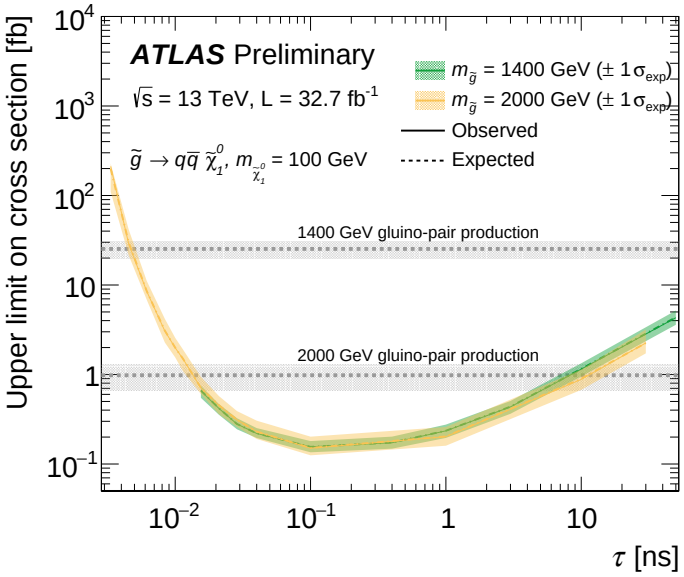

Figure 7: Expected and observed upper 95%-CL cross section limits as a function of gluino lifetime for a neutralino mass of $m_{\tilde{\chi}_1^0} = 100$ GeV. Horizontal lines denote the $\tilde{g}\tilde{g}$ production cross section for various values of $m_{\tilde{g}}$.

Due to an initial underestimation of the sensitivity of the analysis, an inadequate range of signal samples was produced. As a result, the signal efficiency has been extrapolated to gluino masses higher than 2 TeV using a polynomial function validated with available samples.

Upper limits on the gluino mass are also shown as a function of gluino lifetime in Figure 8. DV-level fiducial volume and PV-distance requirements reduce the exclusion power in the high and low extremes of gluino lifetime. For $\tau = 1$ ns, upper limits on the gluino mass are placed above 2.2 TeV for $m_{\tilde{\chi}_1^0} = 100$ GeV.

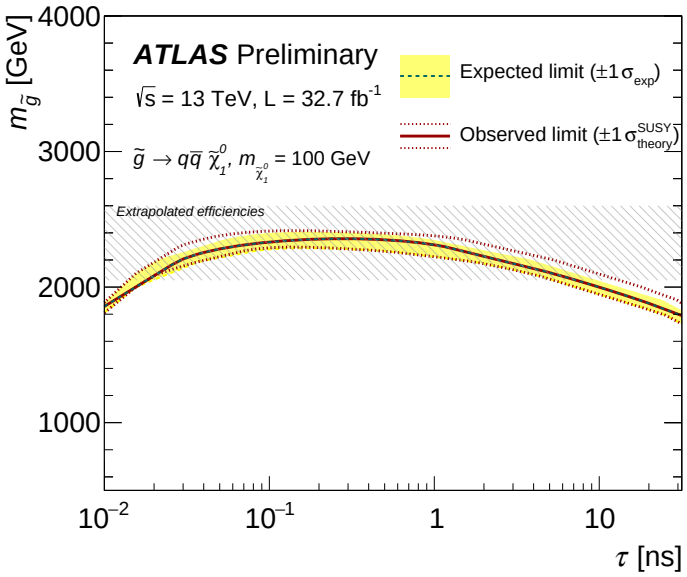

Figure 8: Expected and observed upper limits on the gluino mass are shown as a function of the gluino lifetime for a fixed neutralino mass of 100 GeV. The shaded area indicates the region in which signal efficiencies are estimated by an extrapolation from lower masses.

8 Conclusions

A search for massive, long-lived particles giving rise to displaced multi-track vertices was performed with 32.7 fb^{-1} of pp collisions at $\sqrt{s} = 13$ TeV collected by the ATLAS experiment. The search presented is sensitive to models predicting events with significant $E_{\mathrm{T}}^{\mathrm{miss}}$ and at least one displaced vertex with five or more tracks and a visible invariant mass greater than 10 GeV. With an expected background of 0.02 ± 0.02 events, no events in the data sample were observed in the signal region. With results consistent with the background-only hypothesis, exclusion limits are derived for models predicting the existence of such particles, reaching roughly $m_{\tilde{g}} = 2000$ GeV to 2300 GeV for $m_{\tilde{\chi}_1^0} = 100$ GeV and gluino lifetimes between 0.02 and 10 ns.

Appendix

References

[1] G. Bertone, D. Hooper, and J. Silk, *Particle dark matter: Evidence, candidates and constraints*, Phys. Rept. **405** (2005) 279, arXiv: hep-ph/0404175 [hep-ph].

[2] S. Weinberg, *Implications of Dynamical Symmetry Breaking*, Phys. Rev. **D13** (1976) 974.

[3] L. Susskind, *Dynamics of Spontaneous Symmetry Breaking in the Weinberg-Salam Theory*, Phys. Rev. **D20** (1979) 2619.

[4] S. Dimopoulos, S. Raby, and F. Wilczek, *Supersymmetry and the Scale of Unification*, Phys. Rev. D **24** (1981) 1681.

[5] M. J. Strassler and K. M. Zurek, *Echoes of a hidden valley at hadron colliders*, Phys. Lett. **B651** (2007) 374, arXiv: hep-ph/0604261 [hep-ph].

[6] R. Barbier et al., *R-parity violating supersymmetry*, Phys. Rept. **420** (2005) 1, arXiv: hep-ph/0406039 [hep-ph].

[7] B. C. Allanach et al., *Mass spectrum in R-parity violating minimal supergravity and benchmark points*, Phys. Rev. **D75** (2007) 035002, arXiv: hep-ph/0609263 [hep-ph].

[8] N. Arkani-Hamed and S. Dimopoulos, *Supersymmetric unification without low energy supersymmetry and signatures for fine-tuning at the LHC*, JHEP **06** (2005) 073, arXiv: hep-th/0405159 [hep-th].

[9] G. F. Giudice and A. Romanino, *Split supersymmetry*, Nucl. Phys. B **699** (2004) 65, [Erratum: Nucl. Phys.B706,65(2005)], arXiv: hep-ph/0406088 [hep-ph].

[10] M. Fairbairn et al., *Stable massive particles at colliders*, Phys. Rept. **438** (2007) 1, arXiv: hep-ph/0611040 [hep-ph].

[11] ATLAS Collaboration, *Search for massive, long-lived particles using multitrack displaced vertices or displaced lepton pairs in pp collisions at $\sqrt{s} = 8$ TeV with the ATLAS detector*, Phys. Rev. **D92** (2015) 072004, arXiv: 1504.05162 [hep-ex].

[12] ATLAS Collaboration, *Search for displaced muonic lepton jets from light Higgs boson decay in proton-proton collisions at $\sqrt{s} = 7$ TeV with the ATLAS detector*, Phys. Lett. **B721** (2013) 32, arXiv: 1210.0435 [hep-ex].

[13] ATLAS Collaboration, *Search for non-pointing photons in the diphoton and E_T^{miss} final state in $\sqrt{s}$=7 TeV proton-proton collisions using the ATLAS detector*, Phys. Rev. **D88** (2013) 012001, arXiv: 1304.6310 [hep-ex].

[14] ATLAS Collaboration, *Search for non-pointing and delayed photons in the diphoton and missing transverse momentum final state in 8 TeV pp collisions at the LHC using the ATLAS detector*, Phys. Rev. **D90** (2014) 112005, arXiv: 1409.5542 [hep-ex].

[15] ATLAS Collaboration, *Search for charginos nearly mass-degenerate with the lightest neutralino based on a disappearing-track signature in pp collisions at $\sqrt{(s)}$=8 TeV with the ATLAS detector*, Phys. Rev. **D88** (2013) 112006, arXiv: 1310.3675 [hep-ex].

[16] ATLAS Collaboration, *Search for pair-produced long-lived neutral particles decaying in the ATLAS hadronic calorimeter in pp collisions at* $\sqrt{s} = 8$ *TeV*, Phys. Lett. **B743** (2015) 15, arXiv: 1501.04020 [hep-ex].

[17] ATLAS Collaboration, *Search for long-lived, weakly interacting particles that decay to displaced hadronic jets in proton-proton collisions at* $\sqrt{s} = 8$ *TeV with the ATLAS detector*, Phys. Rev. **D92** (2015) 012010, arXiv: 1504.03634 [hep-ex].

[18] ATLAS Collaboration, *Search for displaced vertices arising from decays of new heavy particles in 7 TeV pp collisions at ATLAS*, Phys. Lett. **B707** (2012) 478, arXiv: 1109.2242 [hep-ex].

[19] ATLAS Collaboration, *Search for long-lived, heavy particles in final states with a muon and multi-track displaced vertex in proton-proton collisions at* $\sqrt{s} = 7$ *TeV with the ATLAS detector*, Phys. Lett. **B719** (2013) 280, arXiv: 1210.7451 [hep-ex].

[20] CMS Collaboration, *Search in leptonic channels for heavy resonances decaying to long-lived neutral particles*, JHEP **02** (2013) 085, arXiv: 1211.2472 [hep-ex].

[21] CMS Collaboration, *Search for Displaced Supersymmetry in events with an electron and a muon with large impact parameters*, Phys. Rev. Lett. **114** (2015) 061801, arXiv: 1409.4789 [hep-ex].

[22] CMS Collaboration, *Search for long-lived particles that decay into final states containing two electrons or two muons in proton-proton collisions at* $\sqrt{s} = 8$ *TeV*, Phys. Rev. **D91** (2015) 052012, arXiv: 1411.6977 [hep-ex].

[23] CMS Collaboration, *Search for Long-Lived Neutral Particles Decaying to Quark-Antiquark Pairs in Proton-Proton Collisions at* $\sqrt{s} = 8$ *TeV*, Phys. Rev. **D91** (2015) 012007, arXiv: 1411.6530 [hep-ex].

[24] CMS Collaboration, *A search for pair production of new light bosons decaying into muons*, Phys. Lett. **B752** (2016) 146, arXiv: 1506.00424 [hep-ex].

[25] CMS Collaboration, *Search for R-parity violating supersymmetry with displaced vertices in proton-proton collisions at sqrt(s) = 8 TeV*, Phys. Rev. D (2016), arXiv: 1610.05133 [hep-ex].

[26] LHCb Collaboration, *Search for long-lived particles decaying to jet pairs*, Eur. Phys. J. **C75** (2015) 152, arXiv: 1412.3021 [hep-ex].

[27] LHCb Collaboration, *Search for hidden-sector bosons in* $B^0 \to K^{*0}\mu^+\mu^-$ *decays*, Phys. Rev. Lett. **115** (2015) 161802, arXiv: 1508.04094 [hep-ex].

[28] LHCb Collaboration, *Search for massive long-lived particles decaying semileptonically in the LHCb detector*, (2016), arXiv: 1612.00945 [hep-ex].

[29] LHCb Collaboration, *Search for long-lived scalar particles in* $B^+ \to K^+\chi(\mu^+\mu^-)$ *decays*, (2016), arXiv: 1612.07818 [hep-ex].

[30] F. Abe et al. (CDF Collaboration), *Search for long-lived parents of* Z^0 *bosons in* $p\bar{p}$ *collisions at* $\sqrt{s} = 1.8$ *TeV*, Phys. Rev. **D58** (1998) 051102, arXiv: hep-ex/9805017 [hep-ex].

[31] V. M. Abazov et al. (D0 Collaboration), *Search for neutral, long-lived particles decaying into two muons in* $p\bar{p}$ *collisions at* $\sqrt{s} = 1.96$*-TeV*, Phys. Rev. Lett. **97** (2006) 161802, arXiv: hep-ex/0607028 [hep-ex].

[32] V. M. Abazov et al. (D0 Collaboration), *Search for Resonant Pair Production of long-lived particles decaying to b anti-b in p anti-p collisions at s**(1/2) = 1.96-TeV*, Phys. Rev. Lett. **103** (2009) 071801, arXiv: 0906.1787 [hep-ex].

[33] J. P. Lees et al. (BaBar Collaboration), *Search for Long-Lived Particles in e^+e^- Collisions*, Phys. Rev. Lett. **114** (2015) 171801, arXiv: 1502.02580 [hep-ex].

[34] D. Liventsev et al. (Belle Collaboration), *Search for heavy neutrinos at Belle*, Phys. Rev. **D87** (2013) 071102, arXiv: 1301.1105 [hep-ex].

[35] A. Heister et al. (ALEPH Collaboration), *Search for gauge mediated SUSY breaking topologies in e^+e^- collisions at center-of-mass energies up to 209-GeV*, Eur. Phys. J. **C25** (2002) 339, arXiv: hep-ex/0203024 [hep-ex].

[36] ATLAS Collaboration, *The ATLAS Experiment at the CERN Large Hadron Collider*, JINST **3** (2008) S08003.

[37] ATLAS Collaboration, *Performance of the ATLAS Trigger System in 2015*, (2016), arXiv: 1611.09661 [hep-ex].

[38] ATLAS Collaboration, *Luminosity determination in pp collisions at $\sqrt{s} = 8$ TeV using the ATLAS detector at the LHC*, Eur. Phys. J. **C76** (2016) 653, arXiv: 1608.03953 [hep-ex].

[39] T. Sjostrand, S. Mrenna, and P. Z. Skands, *PYTHIA 6.4 Physics and Manual*, JHEP **05** (2006) 026, arXiv: hep-ph/0603175 [hep-ph].

[40] ATLAS Collaboration, *Further ATLAS tunes of PYTHIA6 and Pythia 8*, ATL-PHYS-PUB-2011-014 (2011), URL: https://cds.cern.ch/record/1400677.

[41] J. Pumplin et al., *New generation of parton distributions with uncertainties from global QCD analysis*, JHEP **07** (2002) 012, arXiv: hep-ph/0201195 [hep-ph].

[42] G. R. Farrar and P. Fayet, *Phenomenology of the Production, Decay, and Detection of New Hadronic States Associated with Supersymmetry*, Phys. Lett. B **76** (1978) 575.

[43] A. C. Kraan, *Interactions of heavy stable hadronizing particles*, Eur. Phys. J. **C37** (2004) 91, arXiv: hep-ex/0404001 [hep-ex].

[44] W. Beenakker et al., *Squark and gluino production at hadron colliders*, Nucl.Phys. **B492** (1997) 51, arXiv: hep-ph/9610490 [hep-ph].

[45] C. Borschensky et al., *Squark and gluino production cross sections in pp collisions at $\sqrt{s} = 13$, 14, 33 and 100 TeV*, Eur. Phys. J. C **74** (2014) 3174, arXiv: 1407.5066 [hep-ph].

[46] A. Kulesza and L. Motyka, *Soft gluon resummation for the production of gluino-gluino and squark-antisquark pairs at the LHC*, Phys.Rev. **D80** (2009) 095004, arXiv: 0905.4749 [hep-ph].

[47] A. Kulesza and L. Motyka, *Threshold resummation for squark-antisquark and gluino-pair production at the LHC*, Phys.Rev.Lett. **102** (2009) 111802, arXiv: 0807.2405 [hep-ph].

[48] P. M. Nadolsky et al., *Implications of CTEQ global analysis for collider observation*, Phys. Rev. **D78** (2008) 013004, arXiv: 0802.0007 [hep-ph].

[49] A. D. Martin et al., *Parton distributions for the LHC*, Eur. Phys. J. **C63** (2009) 189, arXiv: 0901.0002 [hep-ph].

[50] ATLAS Collaboration, *The ATLAS Simulation Infrastructure*, Eur. Phys. J. **C70** (2010) 823, arXiv: 1005.4568 [physics.ins-det].

[51] S. Agostinelli et al., *GEANT4: A Simulation toolkit*, Nucl. Instrum. Meth. **A506** (2003) 250.

[52] R. Mackeprang and A. Rizzi, *Interactions of Coloured Heavy Stable Particles in Matter*, Eur. Phys. J. **C50** (2007) 353, arXiv: hep-ph/0612161 [hep-ph].

[53] R. Mackeprang and D. Milstead, *An Updated Description of Heavy-Hadron Interactions in GEANT-4*, Eur. Phys. J. **C66** (2010) 493, arXiv: 0908.1868 [hep-ph].

[54] T. Sjostrand, S. Mrenna, and P. Z. Skands, *A Brief Introduction to PYTHIA 8.1*, Comput. Phys. Commun. **178** (2008) 852, arXiv: 0710.3820 [hep-ph].

[55] J. Alwall et al., *The automated computation of tree-level and next-to-leading order differential cross sections, and their matching to parton shower simulations*, JHEP **07** (2014) 079, arXiv: 1405.0301 [hep-ph].

[56] ATLAS Collaboration, *ATLAS Run 1 Pythia8 tunes*, ATL-PHYS-PUB-2014-021 (2014), URL: https://cds.cern.ch/record/1966419.

[57] R. D. Ball et al., *Parton distributions with LHC data*, Nucl. Phys. **B867** (2013) 244, arXiv: 1207.1303 [hep-ph].

[58] ATLAS Collaboration, *Topological cell clustering in the ATLAS calorimeters and its performance in LHC Run 1*, (2016), arXiv: 1603.02934 [hep-ex].

[59] M. Cacciari, G. P. Salam, and G. Soyez, *The anti-k_t jet clustering algorithm*, JHEP **04** (2008) 063, arXiv: 0802.1189 [hep-ph].

[60] ATLAS Collaboration, *Single hadron response measurement and calorimeter jet energy scale uncertainty with the ATLAS detector at the LHC*, Eur. Phys. J. C **73** (2013) 2305, arXiv: 1203.1302 [hep-ex].

[61] ATLAS Collaboration, *Jet energy measurement and its systematic uncertainty in proton–proton collisions at $\sqrt{s}$ = 7 TeV with the ATLAS detector*, Eur. Phys. J. C **75** (2015) 17, arXiv: 1406.0076 [hep-ex].

[62] ATLAS Collaboration, "Performance of missing transverse momentum reconstruction for the ATLAS detector in the first proton-proton collisions at at $\sqrt{s}$= 13 TeV," tech. rep. ATL-PHYS-PUB-2015-027, CERN, 2015, URL: https://cds.cern.ch/record/2037904.

[63] ATLAS Collaboration, *Jet energy scale measurements and their systematic uncertainties in proton-proton collisions at $\sqrt{s}$ = 13 TeV with the ATLAS detector*, (2017), arXiv: 1703.09665 [hep-ex].

[64] ATLAS Collaboration, *Performance of missing transverse momentum reconstruction in proton–proton collisions at $\sqrt{s}$ = 7 TeV with ATLAS*, Eur. Phys. J. C **72** (2012) 1844, arXiv: 1108.5602 [hep-ex].

[65] ATLAS Collaboration, *Performance of algorithms that reconstruct missing transverse momentum in $\sqrt{s}$ = 8 TeV proton–proton collisions in the ATLAS detector*, (2016), arXiv: 1609.09324 [hep-ex].

[66] ATLAS Collaboration, *Track Reconstruction Performance of the ATLAS Inner Detector at $\sqrt{s}$ = 13 TeV*, ATL-PHYS-PUB-2015-018 (2015), URL: https://cds.cern.ch/record/2037683.

[67] S. R. Das, *On a New Approach for Finding All the Modified Cut-Sets in an Incompatibility Graph*, IEEE Trans. Comput. **22** (1973) 187, ISSN: 0018-9340.

[68] ATLAS Collaboration, *A measurement of material in the ATLAS tracker using secondary hadronic interactions in 7 TeV pp collisions*, JINST **11** (2016) P11020, arXiv: 1609.04305 [hep-ex].

[69] A. L. Read, *Presentation of search results: the CL s technique*, Journal of Physics G: Nuclear and Particle Physics **28** (2002) 2693, URL: http://stacks.iop.org/0954-3899/28/i=10/a=313.

[70] M. Baak et al., *HistFitter software framework for statistical data analysis*, Eur. Phys. J. **C75** (2015) 153, arXiv: 1410.1280 [hep-ex].